

Molecular self-assembled monolayers of ruthenium(II)-terpyridine dithiol complex on gold electrode and nanoparticles

Teng-Yuan Dong ^{*}, Chienlin Huang, Chiao-Pei Chen, Ming-Cheng Lin

Department of Chemistry, Center for Nanoscience and Nanotechnology, National Sun Yat-Sen University, Kaohsiung, Taiwan

Received 3 May 2007; received in revised form 12 July 2007; accepted 13 July 2007

Available online 23 August 2007

Abstract

We describe the formation of stable dithiol-bifunctionalized Ru(II)-terpyridine monolayer onto gold electrode. The coverage-dependent behavior onto gold electrode has been studied by electrochemical technique. The stability, surface charge coverage, and electron-transfer kinetics were assessed by cyclic voltammetry. Functionalized monolayer-protected Au clusters (MPCs) were also prepared. The spectroscopic characterization data of MPCs using UV–Vis and TEM techniques are discussed. TEM images showed that functionalized spherical nanoclusters of 4.7 ± 0.3 and 4.3 ± 0.2 nm were produced. The particle sizes are uniform with a narrow size distribution. The morphology of Au(111) metal surface modified with MPCs was imaged using atomic force microscopy (AFM). The nanoparticle layer exhibits a distinct surface morphology, irregularly shaped domains with dimensions from 20 to 60 nm and root mean square heights of 2.401 nm.

© 2007 Elsevier B.V. All rights reserved.

Keywords: Self-assembled monolayers; Nanoparticles; Surface analysis; Adsorption; Chemisorption

1. Introduction

Self-assembled monolayers (SAMs) on metal surfaces have been the subject of extensive research [1]. Much of the recent work is driven by the applications in sensors [2], catalysis [3], molecular and electronic devices [4], and other areas [5]. The fundamental study concerning the structure of the alkanethiols onto gold metal surface has been leading to some interesting developments [6–11]. Tunneling microscopy and diffraction methods have found that SAMs display complex phase behavior that depends upon coverage, temperature, chain length, and method of preparation [6–9]. Long chain alkanethiols are easier to self-assemble on gold surface to form densely packed monolayers that the alkyl chains pack in an all-*trans* conformation

[10]. White and co-workers have studied the coverage-dependent phase behavior of the decanethiolates on Au(111) surface by variable-temperature scanning tunneling microscopy [12]. At the lowest coverage, the surface is composed of a weakly interacting, mobile lattice gas. As coverage and interadsorbate interactions increase, thiolate first condenses into a series of low density striped phases, each with an increasing degree of out-of-phase interdigitation. Finally, the thiol stands up, 30° off normal, in a close-packed saturation phase.

Parallel to this area, the chemistry of nanocomposite materials constitutes a vast field of research, in particular systems including metallic nanoparticles such as gold [13], silver [14], and platinum [15] nanoparticles. These nanoparticles can be regarded as a new class of materials whose properties can be tuned by manipulating the terminal functionalized group, such as alkanethiolate bearing redox-active or photo-active terminal functional group. Many of functionalized monolayer-protected clusters

^{*} Corresponding author. Tel.: +886 7 5253937; fax: +886 7 5253908.
E-mail address: dty@mail.nsysu.edu.tw (T.-Y. Dong).

(MPCs) described to date contain organic and bioorganic ligands such as dendrimers [16] and DNA [17]. Comparatively, the functionalization of MPCs by inorganic system remains much less developed and usually involves alkanethiol chain containing redox-active center. Murray and co-workers have described the preparation of functionalized nanoparticles which are of interest for catalytic applications [18]. Functionalized gold and silver MPCs coated by polypyridyl ruthenium(II) complexes have been reported [13k,19]. Recently, it has been demonstrated that chromophores functionalized nanoparticles are useful in nanophotonic devices and studies have revealed that the optical properties can be tuned by incorporating various photo-active terminal groups [20]. In our group, we investigated the formation of gold nanoparticles comprising both redox-active and photo-active inorganic systems such as 4'-ferrocenyl-2,2':6',2''-terpyridine and 4'-biferrocenyl-2,2':6',2''-terpyridine ruthenium(II)-terpyridyloctanethiolate complexes [21]. The use of such ruthenium(II)-ferrocenyl inorganic complexes in nanocomposite is very promising and should allow combination of physical properties of both molecular complexes and nanoparticles.

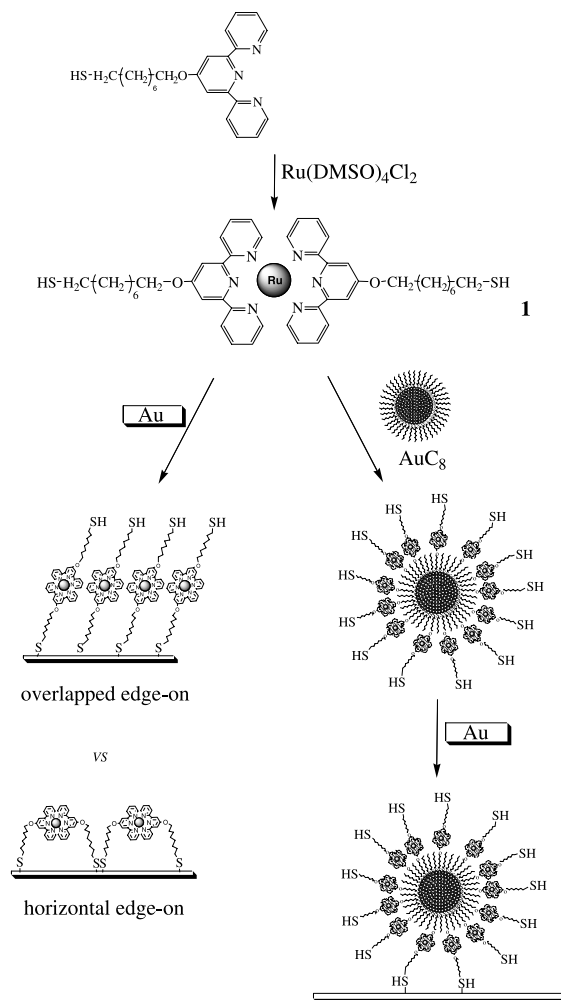
Recently, there has been extensive studies to develop new methodologies for the construction of particle-ordered assemblies [13h,22]. Among them, a bifunctional ligand acts as a linker unit with one end adsorbed onto a substrate surface and the other end used to anchor the particles. This procedure can be repeated many times to build up an arbitrary number of well-defined multilayer structures. Chen and his coworkers reported a study to construct 4-(1-oxo-7-mercaptohexyl)pyridine functionalized gold nanoparticles [23]. The assembling of nanoparticles surface layers was effected by exploiting the complexation interactions between divalent metal ions and pyridine moiety. The number of the nanoparticle layers was controlled by the repetition of the dipping cycles.

Here, we present a system (Scheme 1) based on the preparation of dithiol-bifunctionalized Ru(II)-terpyridine complex (**1**) self-assembled on gold nanoparticles. The coverage-dependent phase behavior of this Ru(II) complex onto gold electrode has been studied by electrochemical measurement. More complex nanostructures based on the covalent attachment of nanoparticles onto gold surface are also described.

2. Experimental

2.1. General information

The preparations involving air sensitive materials were carried out by using standard Schlenk techniques under an inert atmosphere of N₂. Chromatography was performed on neutral Al₂O₃ (act. IV). Dried THF and ether were distilled from Na/benzophenone. All chemicals were reagent grade and used as received. Complex **1** was prepared as illustrated in Scheme 1. Samples of Ru(DM-



Scheme 1.

SO)₄Cl₂ [24] and octanethiolated Au MPCs (AuC₈) were prepared as described by Murray et al. [13b–f].

2.2. Synthesis of 8-(2,2':6',2''-terpyridin-4'-yloxy)octane-1-thiol

Functionalized terpy-thiol was prepared through a similar synthetic route described in our previous paper with some slight modifications [21]. Briefly, the 1,8-diiodooctane was converted to 8-(2,2':6',2''-terpyridin-4'-yloxy)-1-iodooctane by treatment with 4'-hydroxy-terpyridine and K₂CO₃ in acetone, and the resulting solution was then refluxed for 24 h. The halide group was then replaced by treatment with NaSH in THF and refluxed for 8 h under N₂ to create the desired terpy thiol.

2.3. Synthesis of ruthenium(II) complex (**1**)

Complex of **1** (illustrated in Scheme 1) was prepared by reacting 8-(2,2':6',2''-terpyridin-4'-yloxy)octane-1-thiol (0.7800 g, 1.98 mmol) and Ru(DMSO)₄Cl₂ (0.4500 g, 1.00 mmol) in ethanol (40 mL) and refluxing the resulting

solution for 24 h under N_2 . After cooling to room temperature, the volume of the solution was reduced by one half using a rotary evaporator. A saturated aqueous solution of NH_4PF_6 (2 mL) was then added to this dark colored solution to produce a violet precipitate. The violet precipitate was washed several times with ethanol and purified by chromatography. Elution with CH_2Cl_2/CH_3CN (1:1) gave the desired compound with a yield of 35 %. Anal. Calc. for $C_{46}H_{54}F_{12}N_6O_2P_2RuS_2$: C, 46.90; H, 4.59; N, 7.14; S, 5.44. Found: C, 47.39; H, 4.73; N, 6.73; S, 4.76%. 1H NMR (acetone- d_6): δ 0.85–1.41 (m, 6H, CH_2), 1.46 (dt, 2H, CH_2), 1.57 (dt, 2H, CH_2), 1.91 (t, 2H, CH_2), 1.99 (t, 2H, CH_2), 4.90 (dd, 2H, CH_2), 7.37 (t, 2H, tpy- $H_{4,4'}$), 7.71 (d, 2H, tpy- $H_{3,3'}$), 8.08 (t, 2H, tpy- $H_{5,5'}$), 8.78 (s, 2H, tpy- $H_{3',5'}$), 8.86 (d, 2H, tpy- $H_{6,6'}$). Mass spectrum (ESI): M^+ at m/z 1031 ($[M-PF_6]^+$); 443 ($[M-2PF_6]^{2+}$).

2.4. AuC_8 MPCs

Octanethiol-modified Au MPCs were prepared by the method outlined in the literature published by Murray et al. [13b–f]. Briefly, a toluene solution (30 mL) containing octanethiol (1.53 mL, 8.83 mmol) and tetraoctylammonium bromide (TOAB, 0.75 g, 1.37 mmol) was added to an aqueous solution (25 mL) of $HAuCl_4$ (0.15 g, 4.42 mmol). After phase transfer of the $HAuCl_4$ into the toluene had been accomplished, the mixture was reduced with $NaBH_4$ (2.02 g, 53.04 mmol). The organic layer was extracted with toluene. Following the steps of concentrating of the organic layer, pouring into ethanol, standing overnight at $-4^\circ C$, centrifuging and rinsing with ethanol gave the desired Au MPCs. The Au MPCs had average core diameters of approximately ~ 2 nm. These particles were used to induce size and shape evolution with heating treatment in toluene or in TOAB.

2.5. Heating treatment of AuC_8 in toluene (AuC_8-U_t)

Shape evolution with heating treatment in toluene was carried out by the method outlined in the literature published by Zhong et al. [25]. Briefly, particles of AuC_8 were redissolved in a small amount of toluene (2 mL) together with $N(C_8H_{17})_4Br$ (0.2 g). The resulting solution was heated in a silicon oil bath at $145^\circ C$. When the color of this solution changed from brown to dark red, the solution was heated further at $110^\circ C$ for an additional 5 h. The change in color also included a size evolution. The solvent was removed in a rotary evaporator (under $50^\circ C$) followed by washing several times with ethanol and acetone. The Au MPCs created by using the heating treatment had average core diameters of approximately 4.2 ± 0.3 nm (measured by transmission electron microscopy).

2.6. Heating treatment of AuC_8 in TOAB (AuC_8-U_a)

Shape evolution with heating treatment in molten TOAB was carried out by the method outlined in the liter-

ature published by Miyake et al. [26]. Briefly, a toluene solution containing a 2:1 mole ratio of octanethiol to $HAuCl_4$ was reduced using $NaBH_4$ at room temperature following the Murray's procedure. The organic layer was extracted with toluene. Following the evaporation of the organic layer, particles of AuC_8 were heated to $150^\circ C$ with heating rate of $2^\circ C/min$ in a silicon oil bath. After heating at $150^\circ C$ for 30 min, the color of this solution changed from brown to wine-red, the solution was then cooled down to room temperature. The change in color indicates a size evolution. Free thiol and TOAB were removed by rinsing several times with methanol and acetone. The size-evolution Au MPCs (AuC_8-U_a) by heat treatment in TOAB had 3.9 ± 0.2 nm core diameters measured by transmission electron microscopy.

2.7. Synthesis of AuC_8-U_t-1 and AuC_8-U_a-1

A mixture of uniformed Au MPC (AuC_8-U_t or AuC_8-U_a , 65 mg) and **1** (20.0 mg) in 10 mL THF was stirred at room temperature for 48 h. The solvent was removed under vacuum. The resulting product was suspended in a solution of acetone and isolated with centrifuge. This procedure was repeated several times to obtain purified functionalized MPCs (AuC_8-U_t-1 and AuC_8-U_a-1).

2.8. Functionalized gold electrode with **1**, AuC_8-U_t-1 and AuC_8-U_a-1

The functionalized gold electrode was prepared using an Au electrode (0.07 cm^2 geometric area) that was polished with $0.05\ \mu\text{m}$ alumina followed by cleaning with 5% H_2SO_4 and water in a supersonic waver, and then rinsing with water, CH_2Cl_2 and ethanol. Functionalized gold electrode was prepared by soaking Au electrode in a CH_3CN solution of **1** or in a CH_2Cl_2 solution of functionalized gold nanoparticles (AuC_8-U_t-1 or AuC_8-U_a-1) for 24 h. The concentration of **1** was varied from 10^{-2} , 10^{-3} , 10^{-4} , 10^{-5} , 10^{-6} , to 10^{-7} M. The CH_2Cl_2 solution of functionalized gold nanoparticles was prepared by dissolving 30 mg of nanoparticles in 5 mL of CH_2Cl_2 . The electrode was then removed from the adsorption solution after 24 h and washed with CH_2Cl_2 several times.

2.9. Physical methods

The 1H and ^{13}C NMR spectra were run on a Varian UNITY INOVA-500 spectroscopy. The UV spectra were obtained with a Hitachi U-4000 spectroscopy. Transmission electron microscopy (TEM) was performed in JEOL JEM-3010 Analytical Scanning Transmission Electron Microscope. Size and morphology of the nanoparticles were determined by transmission electron microscopy. The nanoparticles dissolved in toluene solution were then dropped into a 200 mesh carbon-coated copper grid sample holder, and then followed by natural evaporation at room temperature.

Cyclic voltammetry was performed using a CHI-600B system. The reference electrode was Ag/AgCl in a saturated KCl solution. The CV measurement for **1** was carried out in a standard three compartments cell under N₂ at 25 °C equipped with a Pt counter electrode, gold working electrode (0.07 cm² geometric area) and Ag/AgCl reference electrode in a CH₂Cl₂/CH₃CN (1:1) solution containing a 0.1 M (*n*-C₄H₉)₄NPF₆ electrolyte. Under these conditions, ferrocene showed a reversible redox process at $E_{1/2}$ = 0.44 V. Electrochemical measurements for functionalized gold electrode were also carried out in a standard cell, using DME as solvent instead of CH₂Cl₂/CH₃CN.

3. Results and discussion

3.1. Synthesis and characterization of **1**

Complex of **1** was prepared by reacting 8-(2,2':6',2''-terpyridin-4'-yloxy)octane-1-thiol (2 equiv.) with 1 equiv. of Ru(DMSO)₄Cl₂. Complex was isolated as the PF₆⁻ salt, purified by column chromatography, and characterized by elemental analysis, 1D and 2D NMR techniques, ESI-MS and UV (given as Supporting information). The NMR characterization of **1** in acetone-*d*₆ was achieved by utilization of ¹H-¹H and ¹H-¹³C COSY and HMBC 2D NMR techniques. The ¹H NMR spectrum of **1** exhibits five signals corresponding to the tpy ligands. The spectrum is characterized by the low-field doublet (appearing at 8.78 ppm) corresponding to the tpy-H_{3',5'} protons and the downer-field doublet (appearing at 8.86 ppm) corresponding to the tpy-H_{6,6'} protons.

The UV-Vis spectral data of **1** and relevant compounds in CH₃CN are given as Supporting information. Transitions occurring in the UV region (λ_{max} at 270 and 310 nm) are ascribed to the ligand-localized nature, mainly of tpy fragments. The visible spectrum for **1** is also dominated by ¹[(d(π)_{Ru})⁶] → ¹[d(π)⁵(π_{tpy}^{*})¹] MLCT absorption band at 480 nm (478 nm; ε = 19800 M⁻¹ cm⁻¹) which is assigned by analogy to the well-documented MLCT transition found for [Ru(tpy)₂]²⁺ (472 nm; ε = 14000 M⁻¹ cm⁻¹) [27]. This absorption band is broad because it includes a series of ¹[(d(π)_{Ru})⁶] → ³[d(π)⁵(π_{tpy}^{*})¹] MLCT transitions which become partially allowed due to the spin-orbital coupling, which has the effect of mixing the singlet and triplet excited-state manifolds [28].

3.2. Electrochemical measurements for **1**

The electrochemical parameters for **1** and related compounds obtained from the CV are summarized in Table 1. As expected, the cyclic voltammograms of **1** and [Ru(tpy)₂]²⁺ are similar [27]. As shown in Fig. 1, the redox behavior in **1** is dominated by the Ru²⁺/Ru³⁺ redox couple ($E_{1/2}$ at 1.22 V). Furthermore, two consecutive reduction waves attributed to the reduction of the Ru(tpy)₂²⁺ core were also observed (tpy/tpy⁻/tpy²⁻ redox couples; $E_{1/2}$ at -1.25 to -1.50 V). Interestingly, we noted that complex

Table 1
CV data of **1** and related compounds with scan rate of 100 mV s⁻¹

Compound	Ru-center		tpy-center	
	$E_{1/2}$ (V) ^a	ΔE_p^b	$E_{1/2}$ (V) ^a	ΔE_p^b
[Ru(tpy) ₂] ²⁺ ^c	1.27		-1.27	
1	1.22	87	-1.25	76
			-1.50	99

^a All half-wave potentials are referred to the Ag/AgCl electrode. Ferrocene shows a reversible one-electron oxidation wave at $E_{1/2}$ = 0.44 V in CH₂Cl₂/CH₃CN (1:1) solution.

^b Peak-to-peak separation between the resolved reduction and oxidation waves maxima.

^c From Ref. [27].

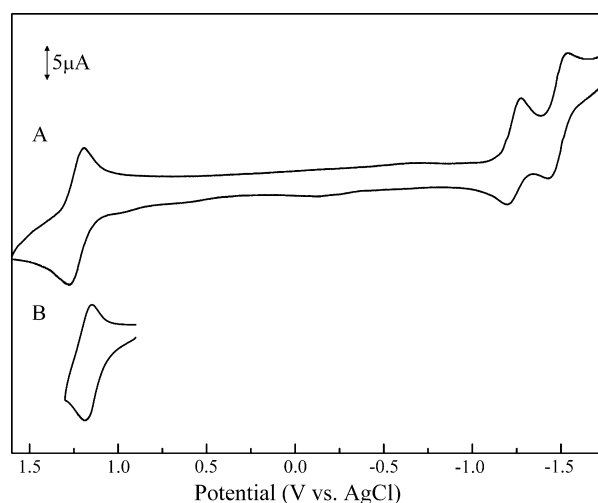


Fig. 1. Cyclic voltammograms of (A) **1**, and (B) soaking Au electrode in a CH₂Cl₂/CH₃CN (1:1) solution of **1** for 3 h. Scan rate = 100 mV s⁻¹.

1 could be adsorbed onto the gold electrode surface. As shown in Fig. 1B, peak-to-peak separation between the resolved reduction and oxidation waves maxima for the Ru²⁺/Ru³⁺ redox couple was reduced from 87 mV to 38 mV by soaking the Au electrode in the CH₂Cl₂/CH₃CN solution of **1** for 3 h. This smaller splitting is consistent with most of current arising from reaction of an adsorbed layer onto the electrode [1]. This interesting observation suggests that complex **1** can be covalently self-assembled onto the gold surface to form monolayer.

3.3. Electrochemical measurement of functionalized electrode

As shown in Fig. 2, the redox behavior of SAM is dominated by the Ru²⁺/Ru³⁺ couple. The stability, surface charge coverage, and electron-transfer mechanism were assessed by cyclic voltammetry. Fig. 2 shows representative cyclic voltammograms of Au electrodes modified by **1** in DME solution. Complete cyclic voltammograms for electrodes soaking in various concentrations of **1** are given as Supporting information. The electrochemical parameters

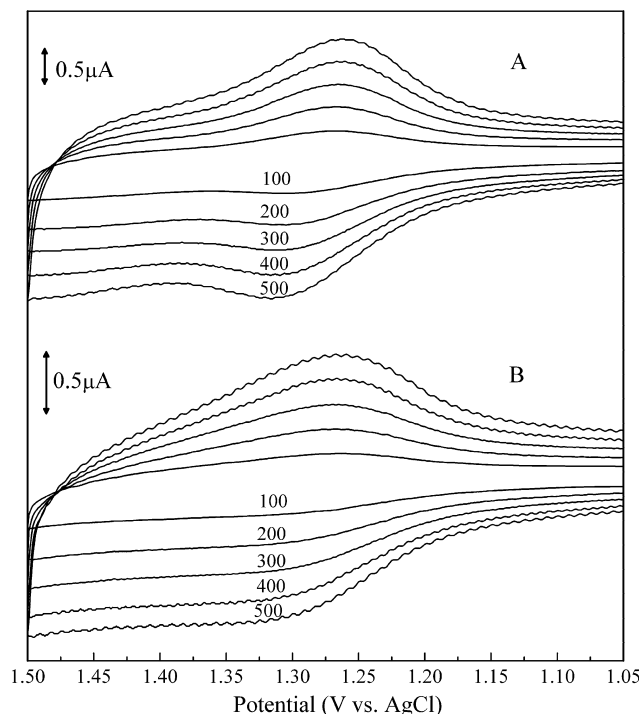


Fig. 2. Cyclic voltammograms in DME for monolayers prepared by soaking Au electrode in 10^{-2} M (A) or 10^{-7} M (B) solutions of **1**. Scan rate = 100–500 mV s^{-1} .

obtained from the CV (ΔE_p , redox peak separation; Γ , surface coverage; k_s , electron-transfer rate constant) are summarized in Tables 2 and 3. Repeat scanning does not change the voltammograms, demonstrating that these monolayers are stable to electrochemical cycling in DME solution.

The pioneered studies of electroactive self-assembled monolayers (SAMs) of ferrocene-terminated alkanethiols coadsorption with unsubstituted *n*-alkanethiols on evapo-

Table 2
Electrochemical data^a extracted from the CV for various modified electrodes with scan rate from 100 to 500 mV s^{-1}

Scan rate	100	200	300	400	500
10^{-2} M ΔE_p	39	42	46	50	53
i_{pc}	0.313	0.560	0.796	1.038	1.271
10^{-3} M ΔE_p	36	44	45	52	56
i_{pc}	0.329	0.571	0.734	0.945	1.165
10^{-4} M ΔE_p	38	42	46	49	54
i_{pc}	0.295	0.487	0.704	0.903	1.076
10^{-5} M ΔE_p	39	42	47	52	55
i_{pc}	0.208	0.371	0.538	0.660	0.825
10^{-6} M ΔE_p	18	24	28	31	35
i_{pc}	0.190	0.349	0.510	0.644	0.824
10^{-7} M ΔE_p	11	21	25	31	34
i_{pc}	0.166	0.281	0.445	0.556	0.679

^a Scan rate, ΔE_p (redox peak-to-peak separation), and i_{pc} (current of cathodic peak) are in units of mV s^{-1} , mV and μA , respectively.

Table 3
Surface coverage (Γ) and standard electron-transfer rate constant (k_s) calculated from CV with scan rate of 100 mV s^{-1} for modified electrode

Concentration (M)	10^{-2}	10^{-3}	10^{-4}	10^{-5}	10^{-6}	10^{-7}
Q_{Ru} (C, $\times 10^8$) ^a	14.9	14.7	14.3	7.1	6.8	3.4
Γ (mol/cm^2 , $\times 10^{12}$) ^b	21.9	21.6	21.0	10.3	9.9	6.5
ΔE_p (mV) ^c	39	36	38	39	18	11
k_s (s^{-1})	3.4	3.7	3.5	3.4	7.8	11.5

^a Surface charge.

^b $\Gamma = Q_{Ru}/nFA$ ($A = 0.07 \text{ cm}^2$).

^c Peak-to-peak separation between the resolved reduction and oxidation waves maxima.

rated gold films were reported by Chidsey et al. [1g]. Monolayers containing low concentrations (mole fraction (χ_{Fc}) ≤ 0.25) of alkanethiols linked to ferrocene by a polar ester group ($\text{FcCO}_2(\text{CH}_2)_n\text{SH}$) coadsorption with $\text{CH}_3(\text{CH}_2)_n\text{SH}$, ($n = 7, 9, 11$) show thermodynamically ideal surface electrochemistry. At low mole fraction, the oxidation and reduction peaks are symmetric and with no splitting between the oxidation and reduction peaks. The lack of peak splitting indicates that the rate of electron transfer is rapid on the time scale of the electrochemical experiment. Chidsey suggested that the ferrocene groups to be homogeneous and noninteracting. At higher mole fractions of the electroactive thiol in the adsorption solution, the resulting cyclic voltammograms broaden, develop an asymmetry, and finally develop an additional set of peaks as the amount of ferrocene is increased. Chidsey suggested that the breakdown of the thermodynamically ideal behavior of this system is probably due to a combination of interaction between ferrocene sites and inhomogeneity of those sites at higher surface coverages. Use of ferrocene-terminated thiols ($\text{Fc}(\text{CH}_2)_{11}\text{SH}$) in which the ferrocene is attached directly to the polymethylene chain without a polar ester group leads to broadened electrochemical features, even at the lowest fraction ($\chi_{Fc} = 0.05$) examined. This highly nonideal behavior at low surface coverage suggests a strong interaction between the ferrocene groups, perhaps due to aggregation.

In our case, at higher molar concentrations of the electroactive dithiol (**1**) in the adsorption solution, the resulting cyclic voltammograms are symmetric and with small splitting between the oxidation and reduction peaks. As shown in Fig. 3, the peak current of i_{pc} is proportional to the scan rate (v), in contrast to the $v^{1/2}$ dependence observed for Nernstian waves of diffusing species [29]. Decreasing the concentrations of **1** in the adsorption solution, such as 10^{-5} – 10^{-7} M, results in very similar cyclic voltammograms with smaller splitting between the oxidation and reduction peaks.

As given in Table 3, the splitting between the oxidation and reduction peaks corresponds to a standard electron-transfer rate constant (k_s) [30,31]. Value of k_s is conveniently determined by monitoring the peak separation of the CV wave. Results are given in Table 3, assuming $\alpha = 0.5$ [30]. Data calculated using Laviron's formalism

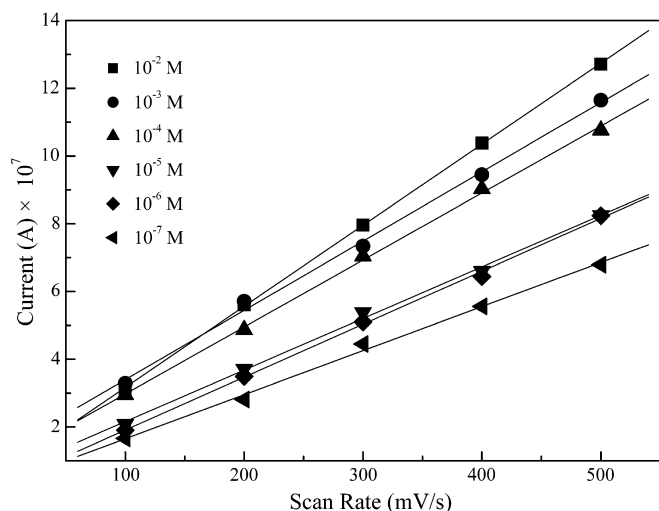


Fig. 3. Peak current of i_{pc} vs. scan rate.

[31] for higher molar concentrations (10^{-2} – 10^{-5} M) is well constant, corresponding to a standard electron-transfer rate constant of $\sim 3.5 \text{ s}^{-1}$. At concentrations of 10^{-6} and 10^{-7} M, standard electron-transfer rate constant is significantly increased. For 10^{-7} M adsorption solution, the voltammogram shows a peak splitting of 11 mV with scan rate of 100 mV s^{-1} . This splitting corresponds to a standard electron-transfer rate constant of 11.5 s^{-1} . In our study, we do not suggest the presence of ohmic errors, since a systematic decrease of k_s at higher sweep rates is not found. Ohmic error is not obvious in our study. The maximum peak current in the voltammogram at the highest sweep rate (500 mV s^{-1}) is $\sim 1.3 \mu\text{A}$ in the case of 10^{-2} M. Ohmic losses are small enough that they may be ignored. The minimum ohmic error occurs at the lowest sweep rate, for which the current is minimum. Therefore, standard electron-transfer rate constant was calculated based on the voltammogram with the scan rate of 100 mV s^{-1} .

The amount of electroactive centers in the monolayers can be calculated from the cyclic voltammograms. The area under the peaks was integrated and divided by the scan rate to obtain the amount of charge passed to the $\text{Ru}^{2+}/\text{Ru}^{3+}$ sites. The surface charge densities ($\mu\text{C}/\text{cm}^2$) obtained by this procedure are converted to Ru(II) complex surface coverages by dividing by the electron charge. Fig. 4 shows Ru(II) complex surface coverages plotted vs the molar concentrations of **1**. The surface coverages of electroactive Ru(II) centers are smaller than the maximum theoretical value ($1.5 \times 10^{-10} \text{ mole cm}^{-2}$) calculated for a close-packed monolayer of Ru(II) complexes with 0.98 nm^2 projection area [32]. As shown in Fig. 4, the surface coverages of the electrodes modified by immersion in more concentrated solutions are well constant ($\sim 21.5 \times 10^{-12} \text{ mol}/\text{cm}^2$). The constancy of surface coverage on the gold surface holds with the concentrations of adsorption solutions from 10^{-2} to 10^{-4} M at 25°C . However, at concentration of 10^{-7} M, the surface coverage is decreased drastically to

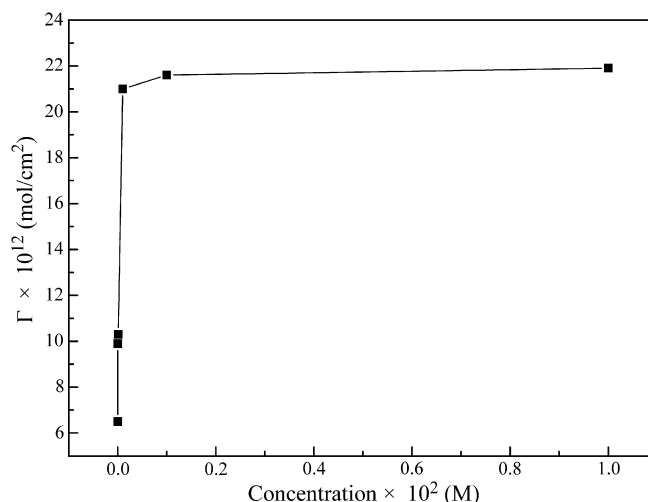


Fig. 4. Ru(II) complex surface coverages vs. the molar concentrations of **1**.

$6.5 \times 10^{-12} \text{ mol}/\text{cm}^2$ at 25°C . The influence of temperature was not systematically investigated in this work; hence, the modified electrodes reported here were formed at room temperature. Constancy of surface coverage in more concentrated solutions (10^{-2} – 10^{-4} M) can, at least in part, be explained by the formation of saturated SAM. For concentrations from 10^{-5} to 10^{-7} M, surface coverages are decreased drastically and the decreasing of surface coverages can be explained by the formation horizontal edge-on orientation SAM.

As mentioned in the section of introduction, SAMs display complex phase behavior that depends upon coverage, temperature, chain length, and method of preparation [6–9]. The difference of redox peak-to-peak separation (ΔE_p), surface coverage, and electron-transfer rate constant for various SAMs prepared by soaking Au electrode in different concentration of **1** can be attributed to the structural difference between overlapped edge-on and horizontal edge-on orientations, as shown in Scheme 1. In present study, the surface coverage is lower for the horizontal edge-on orientation resulting in faster electron-transfer kinetics, compared with the overlapped edge-on orientation.

3.4. Characterizations of $\text{AuC}_8\text{-U}_r\text{-1}$ and $\text{AuC}_8\text{-U}_a\text{-1}$ MPCs

The functionalized MPCs were characterized by TEM for particle size and shape, and UV–Vis spectroscopy (given as Supporting information). As shown in Fig. 5, our TEM data of MPCs showed average core sizes of 4.7 ± 0.3 and $4.3 \pm 0.2 \text{ nm}$ for $\text{AuC}_8\text{-U}_r\text{-1}$ and $\text{AuC}_8\text{-U}_a\text{-1}$ MPCs, respectively. The particle sizes appear uniform with a narrow distribution. Optically, both intensity and energy of the surface plasmon (SP) resonance bands of nanoparticles are known to be strongly dependent on size [13b]. Spectra of $\text{AuC}_8\text{-U}_r\text{-1}$ and $\text{AuC}_8\text{-U}_a\text{-1}$ showed identifiable SP bands at 515 nm.

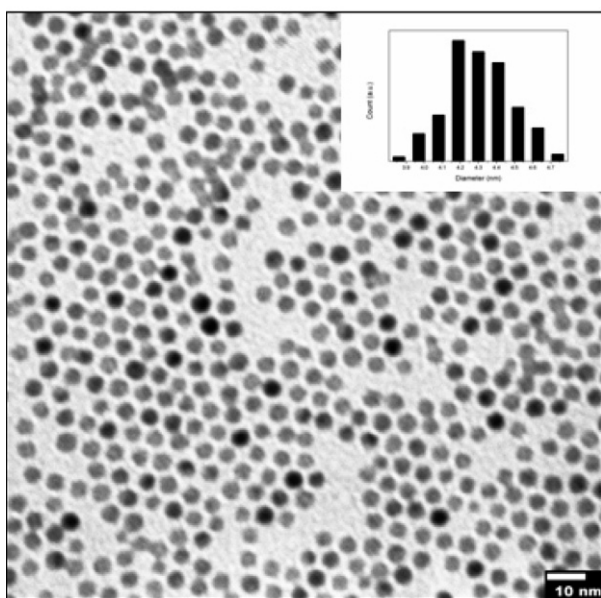
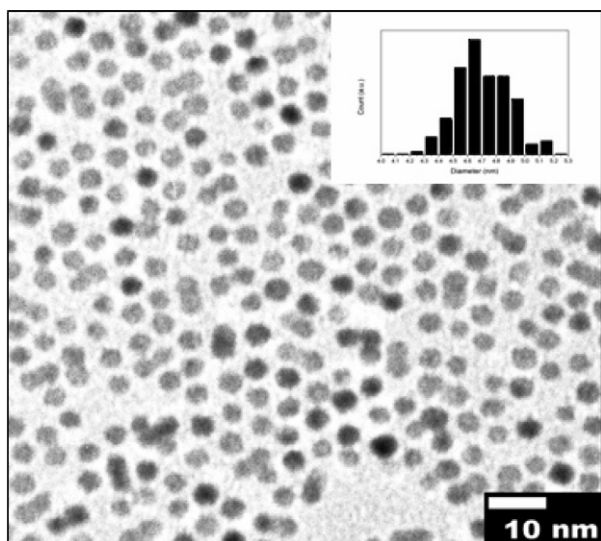


Fig. 5. TEM images of $\text{AuC}_8\text{-U}_t\text{-1}$ (top) and $\text{AuC}_8\text{-U}_a\text{-1}$ (bottom) with histograms showing the respective size distribution.

3.5. Electrochemical measurements of electrode modified with MPCs

Cyclic voltammograms for electrode modified with $\text{AuC}_8\text{-U}_t\text{-1}$ and $\text{AuC}_8\text{-U}_a\text{-1}$ MPCs are shown in Fig. 6. The electrochemical parameters are summarized in Table 4. As expected, one reversible redox wave was observed, the peak current is proportional to the potential scan rate, and the wave shape is symmetrical. The peak-to-peak separation is smaller than 59 mV expected for diffusing electron-transfer kinetics [29]. Electrochemical factors suggest that gold electrode can be functionalized by $\text{AuC}_8\text{-U}_t\text{-1}$ and $\text{AuC}_8\text{-U}_a\text{-1}$ MPCs.

The morphology of Au(111) metal surface modified with $\text{AuC}_8\text{-U}_a\text{-1}$ MPC was imaged using atomic force microscopy (AFM). The nanoparticle layer exhibits a dis-

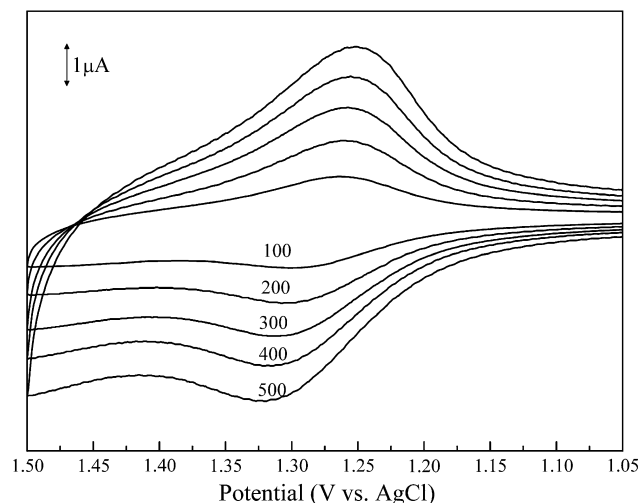


Fig. 6. Cyclic voltammograms in DME for modified electrode prepared by soaking Au electrode in a solution of $\text{AuC}_8\text{-U}_a\text{-1}$. Scan rate = 100–500 mV s^{-1} .

Table 4

Electrochemical data extracted from the CV for $\text{AuC}_8\text{-U}_a\text{-1}$ modified electrode with scan rate from 100 to 500 mV s^{-1}

Scan rate (mV s^{-1})	$E_{1/2}^a$	ΔE_p^b	$i_{pc} \times 10^7$ (A^c)
100	1.28	37	6.98
200	1.28	46	12.63
300	1.28	57	17.39
400	1.28	59	22.01
500	1.28	69	26.26

^a Half-wave potential.

^b Redox peak-to-peak separation.

^c Current of cathodic peak.

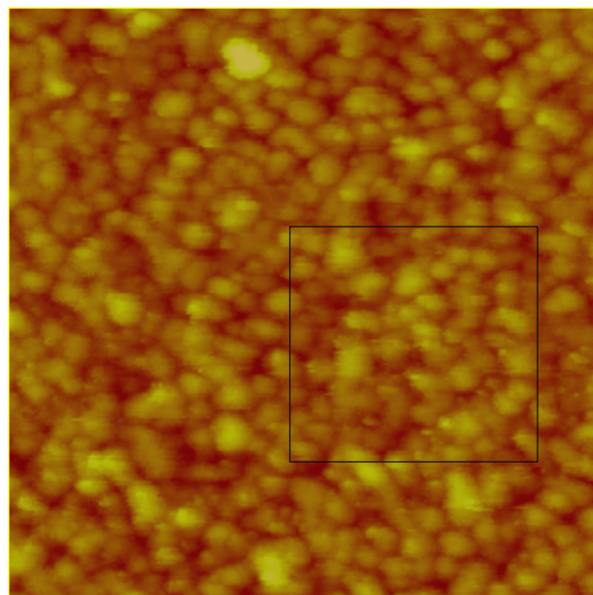


Fig. 7. Topographic AFM image ($1.0 \times 1.0 \mu\text{m}^2$) of covalent attachment of $\text{AuC}_8\text{-U}_a\text{-1}$ nanoparticles onto Au(111) surface.

tinct surface morphology, as shown in Fig. 7, irregularly shaped domains with dimensions from 20 to 60 nm and root mean square heights of 2.401 nm. The measured height possibly suggests a layer of AuC₈-U_a-1 MPC. The morphology of layer is not homogeneous, partly due to the presence of three dimensional clusters and the coexistence of various orientations.

4. Conclusion

We have prepared bifunctionalized Ru(II)-dithiol complex. Spectroscopic results show that this complex is versatile in building molecular self-assembled monolayers on gold surface and gold clusters. The stability, surface charge coverage, and electron-transfer kinetics were assessed by cyclic voltammetry. Well constant standard electron-transfer rate constants for higher molar concentrations (10^{-2} – 10^{-5} M), calculated from the redox peak separation of the CV wave, suggest the formation of saturated overlapped edge-on orientation SAM. At lower concentrations (10^{-6} – 10^{-7} M), the surface coverage is lower and the formation of horizontal edge-on orientation SAM results in faster electron-transfer kinetics. Uniform functionalized monolayer-protected Au clusters were also prepared. Complex of **1** can act as a bifunctionalized linker with one end adsorbed onto the gold surface and the other end used to anchor the gold nanoparticle. Atomic force microscopy shows that the nanoparticle layer exhibits a distinct surface morphology, irregularly shaped domains with dimensions from 20 to 60 nm.

Acknowledgements

Our work was generously supported by the National Science Council (NSC92-2113-M-110-011), Taiwan, ROC, and Department of Chemistry and Center for Nanoscience and Nanotechnology at Sun Yat-Sen University.

Appendix A. Supplementary material

The UV–Vis and ESI-mass spectra of **1**, complete cyclic voltammograms in DME for monolayers prepared by soaking Au electrode in solution of **1** with different concentration, and UV–Vis spectra of AuC₈-U_r-**1** and AuC₈-U_a-**1** are included. Supplementary data associated with this article can be found, in the online version, at doi:10.1016/j.jorgchem.2007.07.055.

References

- [1] (a) A. Ulman, Chem. Rev. 96 (1996) 1533–1554; (b) T.L. Brower, M. Cook, A. Ulman, J. Phys. Chem. B 107 (2003) 11721–11725; (c) E. Delamarche, B. Michel, H.A. Biebuyck, C. Gerber, Adv. Mater. 8 (1996) 719–729; (d) J.B. Schlenoff, M. Li, H. Ly, J. Am. Chem. Soc. 117 (1995) 12528–12536; (e) J. Xu, H.-L. Li, J. Colloid Interf. Sci. 176 (1995) 138–149;
- (f) D.M. Collard, M.A. Fox, Langmuir 7 (1991) 1192–1197;
- (g) C.E.D. Chidsey, C.R. Bertozzi, T.M. Putvinski, A.M. Majsce, J. Am. Chem. Soc. 112 (1990) 4301–4306;
- (h) R.S. Ingram, M.J. Hostetler, R.W. Murray, T.G. Schaaf, J.T. Khoury, R.L. Whetten, T.P. Bigioni, D.K. Guthrie, P.N. First, J. Am. Chem. Soc. 119 (1997) 9279–9280;
- (i) S. Chen, R.S. Ingram, M.J. Hostetler, J.J. Pietron, R.W. Murray, T.G. Schaaff, J.T. Khoury, M.M. Alvarez, R.L. Whetten, Science 280 (1998) 2098–2101;
- (j) A.S. Viana, L.M. Abrantes, G. Jin, S. Floate, R.J. Nichols, M. Kalaji, Phys. Chem. Chem. Phys. 3 (2001) 3411–3419;
- (k) L. Zhang, L.A. Godinez, T. Lu, G.W. Gokel, A.E. Kaifer, Angew. Chem., Int. Ed. Engl. 34 (1995) 235–237;
- (l) Q. Zhang, L.A. Archer, J. Phys. Chem. B 107 (2003) 13123–13132;
- (m) S.J. Green, J.J. Stokes, M.J. Hostetler, J.J. Pietron, R.W. Murray, J. Phys. Chem. B 101 (1997) 2663–2668.
- [2] (a) K.W. Gano, D.C. Myles, Tetrahedron Lett. 41 (2000) 4247–4250; (b) M.T. Rojas, A.E. Kaifer, J. Am. Chem. Soc. 117 (1995) 5883–5884; (c) S. Bharathi, V. Yegnaraman, G.P. Rao, Langmuir 11 (1995) 666–668.
- [3] (a) M. Peter, X.-M. Li, J. Huskens, D.N. Reinhoudt, J. Am. Chem. Soc. 126 (2004) 11684–11690; (b) D. Rautaray, K. Sinha, S.S. Shankar, S.D. Adyanthaya, M. Sastry, Chem. Mater. 16 (2004) 1356–1361; (c) K.K. Ashok, Chem. Rev. 102 (2002) 3579–3588; (d) V. Chechik, R.M. Crooks, C.J.M. Stirling, Adv. Mater. 12 (2000) 1161–1171.
- [4] (a) S. Steinberg, Y. Tor, E. Sabatini, I. Rubinstein, J. Am. Chem. Soc. 113 (1991) 5176–5182; (b) J.J. Hickmann, D. Ofer, P.E. Laibinis, G.M. Whitesides, M.S. Wrighton, Science 252 (1991) 688–691; (c) M.O. Wolf, M.A. Fox, J. Am. Chem. Soc. 117 (1995) 1845–1846; (d) M. Daniel, D. Astruc, Chem. Rev. 104 (2004) 293–346; (e) K.L. Kelly, E. Coronado, L.L. Zhao, G.C. Schatz, J. Phys. Chem. B 107 (2003) 668–677; (f) D.I. Gittins, D. Bethell, D.J. Schiffrin, R.J. Nichols, Nature 408 (2000) 67–69; (g) M.A. Hayat (Ed.), Colloidal Gold: Principles, Methods, and Applications, Academic Press, San Diego, 1991; (h) A.P. Alivisatos, Science 271 (1996) 933–937; (i) G. Schmid, Chem. Rev. 92 (1992) 1709–1727; (j) S. Peschel, G. Schmid, Angew. Chem., Int. Ed. Engl. 34 (1995) 1442–1443; (k) A. Duteil, G. Schmid, J. Chem. Soc., Chem. Commun. (1995) 31–32; (l) C. Petit, P. Lixon, M.P. Pileni, J. Phys. Chem. 97 (1993) 12974–12983; (m) M.P. Pileni, Langmuir 13 (1997) 3266–3276; (n) L.M. Lizmarzan, M. Giersig, P. Mulvaney, Langmuir 12 (1996) 4329–4335.
- [5] (a) A.A. Gewirth, B.K. Niece, Chem. Rev. 97 (1997) 1129–1162; (b) F.P. Zamborini, R.M. Crooks, Langmuir 14 (1998) 3279–3286; (c) E. Schmidt, W. Schurig, W. Sellschopp, Tech. Mech. Thermodyn. 1 (1930) 53–63; (d) B. Sellergren, A. Swietlow, T. Arnebrant, K.K. Unger, Anal. Chem. 68 (1996) 402–407; (e) F. Auer, D.W. Schubert, M. Stamm, T. Arnebrant, A. Swietlow, M. Zizlsperger, B. Sellergren, Chem. Eur. J. 5 (1999) 1150–1159.
- [6] E.U.T. van Velzen, J.F.J. Engbersen, P.J. de Lange, J.W.G. Mahy, D.N. Reinhoudt, J. Am. Chem. Soc. 117 (1995) 6853–6862.
- [7] L.H. Dubois, R.G. Nuzzo, Annu. Rev. Phys. Chem. 43 (1992) 437–463.
- [8] P. Fenter, A. Eberhardt, P. Eisenberger, Science 266 (1994) 1216–1217.
- [9] G.E. Poirier, Langmuir 15 (1999) 1167–1175.
- [10] (a) R.G. Nuzzo, L.H. Dubois, D.L. Allara, J. Am. Chem. Soc. 112 (1990) 558–569; (b) C.E.D. Chidsey, D.N. Loiacono, Langmuir 6 (1990) 682–691.

- [11] (a) C.E.D. Chidsey, G.-Y. Liu, P. Rowntree, G. Scoles, *J. Chem. Phys.* 91 (1989) 4421–4423;
(b) L. Strong, G.M. Whitesides, *Langmuir* 4 (1988) 546–558.
- [12] W.P. Fitts, J.M. White, G.E. Poirter, *Langmuir* 18 (2002) 2096–2102.
- [13] (a) K. Uosaki, Y. Sato, H. Kita, *Langmuir* 7 (1991) 1510–1514;
(b) R.H. Terrill, T.A. Postlethwaite, C.-H. Chen, C.-D. Poon, A. Terzis, A. Chen, J.E. Hutchison, M.R. Clark, G. Wignall, J.D. Londono, R. Superfine, M. Falvo, C.S. Johnson, E.T. Samulski, R.W. Murray, *J. Am. Chem. Soc.* 117 (1995) 12537–12548;
(c) M.J. Hostetler, J. Wingate, C.-J. Zhong, J.E. Harris, R.W. Vachet, M.R. Clark, J.D. Londono, S.J. Green, J.J. Stokes, G.W. Wignall, G.L. Glish, M.D. Porter, N.D. Evans, R.W. Murray, *Langmuir* 14 (1998) 17–30;
(d) S.J. Green, J.J. Pietron, J.J. Stokes, M.J. Hostetler, H. Vu, W.P. Wuefing, R.W. Murray, *Langmuir* 14 (1998) 5612–5619;
(e) M. Brust, M. Walker, D. Bethell, D.J. Schiffrin, R. Whyman, *J. Chem. Soc., Chem. Commun.* (1994) 801–802;
(f) M. Brust, J. Fink, D. Bethell, D.J. Schiffrin, C.J. Kiely, *J. Chem. Soc., Chem. Commun.* (1995) 1655–1656;
(g) A. Kumar, S. Mandal, P.R. Selvakannan, R. Pasricha, A.B. Mandale, M. Sastry, *Langmuir* 19 (2003) 6277–6282;
(h) S. Chen, *J. Phys. Chem. B* 104 (2000) 663–667;
(i) S.D. Bunge, T. Boyle, T. Headley, *NanoLetter* 3 (2002) 901–905;
(j) K.S. Mayya, F. Caruso, *Langmuir* 19 (2003) 6987–6993;
(k) T.B. Norsten, B.L. Frankamp, V.M. Rotello, *NanoLetter* 2 (2002) 1345–1348.
- [14] (a) X.Z. Lin, X. Teng, H. Yang, *Langmuir* 19 (2003) 10081–10085;
(b) W. Wang, S. Efrima, O. Regev, *Langmuir* 14 (1998) 602–610;
(c) N. Yang, K. Aoki, *J. Phys. Chem. B* 109 (2005) 23911–23917;
(d) W. Wang, X. Chen, S. Efrima, *J. Phys. Chem. B* 103 (1999) 7238–7246;
(e) Y. Wang, J.F. Wong, X. Teng, X.Z. Lin, H. Yang, *NanoLetter* 3 (2003) 1555–1559;
(f) X.Z. Lin, A.D. Terepka, H. Yang, *NanoLetter* 4 (2004) 2227–2232.
- [15] (a) D.-Q. Yang, B. Hennequin, E. Sacher, *Chem. Mater.* 18 (2006) 5033–5038;
(b) N.M. Markovic, T.J. Schmidt, V. Stamenkovic, P.N. Ross, *Fuel Cells* 1 (2001) 105–116;
(c) H. Ye, R.M. Crooks, *J. Am. Chem. Soc.* 127 (2005) 4930–4934;
(d) M. Arenz, K.J.J. Mayrhofer, V. Stamenkovic, B.B. Blizanac, T. Tomoyuki, P.N. Ross, N.M. Markovic, *J. Am. Chem. Soc.* 127 (2005) 6819–6829.
- [16] (a) G.R. Newkome, E. He, L.A. Godinez, *Macromolecules* 31 (1998) 4382–4386;
(b) U.S. Schubert, C.H. Weidl, C.N. Moorefield, G.R. Baker, G.R. Newkome, *Polym. Prep.* 40 (1999) 940–941;
(c) R.M. Crooks, B.L. Lemon, L. Sun, L.K. Yeung, M. Zhao, *Top. Curr. Chem.* 212 (2001) 81–135;
(d) R.M. Crooks, M. Zhao, L. Sun, V. Chechik, L.K. Yeung, *Acc. Chem. Res.* 34 (2001) 181–190;
(e) O.M. Wilson, R.W.J. Scott, J.C. Garcia-Martinez, R.M. Crooks, *J. Am. Chem. Soc.* 127 (2005) 1015–1024.
- [17] (a) A.T. Daniher, J.K. Bashkin, *Chem. Commun.* (1998) 1077–1078;
(b) R. Elghanian, J.J. Storhoff, R.C. Mucic, R.L. Letsinger, C.A. Mirkin, *Science* 277 (1997) 1078–1081;
(c) C.A. Mirkin, R.L. Letsinger, R.C. Mucic, J.J. Storhoff, *Nature* 382 (1996) 607–609.
- [18] (a) R.S. Ingram, M.J. Hostetler, R.W. Murray, *J. Am. Chem. Soc.* 119 (1997) 9175–9178;
(b) M.J. Hostetler, S.J. Green, J.J. Stokes, R.W. Murray, *J. Am. Chem. Soc.* 118 (1996) 4212–4213.
- [19] (a) C.R. Mayer, E. Dumas, F. Secheresse, *Chem. Commun.* (2005) 345–347;
(b) M. Ito, T. Tsukatani, H.J. Fujihara, *Mater. Chem.* 15 (2005) 960–964;
- (c) U.S. Schubert, C. Eschbaumer, O. Hien, P. Andres, *Tetrahedron Lett.* 42 (2001) 4705–4707;
(d) M. Maskus, H. Abruna, *Langmuir* 12 (1996) 4455–4462;
(e) N. Terasaki, T. Akiyama, S. Yamada, *Langmuir* 18 (2002) 8666–8671.
- [20] (a) K.G. Thomas, P.V. Kamat, *Acc. Chem. Res.* 36 (2003) 888–898;
(b) B.I. Ipe, K.G. Thomas, *J. Phys. Chem. B* 108 (2004) 13265–13272;
(c) F. Stellacci, C.A. Bauer, T. Meyer-Friedrichsen, W. Wenseleers, S.R. Marder, J.W. Perry, *J. Am. Chem. Soc.* 125 (2003) 328–329;
(d) M.M.Y. Chen, A. Katz, *Langmuir* 18 (2002) 2413–2420;
(e) E. Dulkeith, A.C. Morteani, T. Niedereichholz, T.A. Klar, J. Feldmann, S.A. Levi, F.C.J.M. van Veggel, D.N. Reinhoudt, M. Moller, D.I. Gittins, *Phys. Rev. Lett.* 89 (2002) 203002-1–203002-4;
(f) H. Imahori, M. Arimura, T. Hanada, Y. Nishimura, I. Yamazaki, Y. Sakata, S. Fukuzumi, *J. Am. Chem. Soc.* 123 (2001) 335–336.
- [21] (a) T.-Y. Dong, H.W. Shih, L.S. Chang, *Langmuir* 20 (2004) 9340–9347;
(b) T.-Y. Dong, L.S. Chang, I.M. Tseng, S.J. Huang, *Langmuir* 20 (2004) 4471–4479;
(c) H.W. Shih, T.-Y. Dong, *Inorg. Chem. Chem. Commun.* 7 (2004) 646–649.
- [22] (a) F. Auer, M. Scotti, A. Ulman, R. Jordan, B. Sellergren, J. Garno, G.Y. Liu, *Langmuir* 16 (2000) 7554–7557;
(b) M. Brust, D. Bethell, C.J. Kiely, D. Schiffrin, *Langmuir* 14 (1998) 5425–5429;
(c) D. Gittins, D. Bethell, R.J. Nichols, D. Schiffrin, *J. Mater. Chem.* 10 (2000) 79–83.
- [23] S. Chen, R. Pei, T. Zhao, D.J. Dyer, *J. Phys. Chem. B* 106 (2002) 1903–1908.
- [24] (a) R. Ziessel, V. Grossshenny, M. Hissler, C. Stroh, *Inorg. Chem.* 43 (2004) 4262–4271;
(b) M. Gal, C. Marzin, G. Tarrago, I. Zidane, T. Hours, D. Lerner, C. Andrieux, H. Gampp, J.M. Saveant, *Inorg. Chem.* 25 (1986) 1775–1778;
(c) D.N. Marks, W.O. Siegl, R.R. Gagne, *Inorg. Chem.* 21 (1982) 3140–3147.
- [25] M.M. Maye, W. Zheng, F.L. Leibowitz, N.K. Ly, C.J. Zhong, *Langmuir* 16 (2000) 490–497.
- [26] T. Shimizu, T. Teranishi, S. Hasegawa, M. Miyake, *J. Phys. Chem. B* 107 (2003) 2719–2724.
- [27] (a) K. Hutchison, J.C. Morris, T.A. Nile, J.L. Walsh, D.W. Thompson, J.D. Petersen, J.R. Schoonover, *Inorg. Chem.* 38 (1999) 2516–2523;
(b) J.N. Braddock, T.J. Meyer, *J. Am. Chem. Soc.* 95 (1973) 3158–3162.
- [28] (a) E.M. Kober, T.J. Meyer, *Inorg. Chem.* 21 (1982) 3967–3977;
(b) B.J. Coe, D.W. Thompson, C.T. Culbertson, J.R. Schoonover, T.J. Meyer, *Inorg. Chem.* 34 (1995) 3385–3395.
- [29] R.W. Murray, in: A.J. Bard (Ed.), *Electroanalytical Chemical*, vol. 13, Marcel Dekker, New York, 1984, pp. 191–368.
- [30] Standard rate constants are calculated as recommended by Laviron assuming $\alpha = 0.5$.
- [31] (a) E. Laviron, *J. Electroanal. Chem.* 101 (1979) 19–28;
(b) S. Creager, C.J. Yu, C. Bamdad, S. O’Conner, T. MacLean, E. Lam, Y. Chong, G.T. Olsen, J. Luo, M. Gozin, J.F. Kaysyem, *J. Am. Chem. Soc.* 121 (1999) 1059–1064;
(c) K. Weber, L. Hockett, S. Creager, *J. Phys. Chem. B* 101 (1997) 8286–8291.
- [32] W.C. Bigelow, D.L. Pickett, W.A. Zisman, *J. Colloid Interf. Sci.* 1 (1946) 513–538.